PHYSICAL REVIEW B VOLUME 22, NUMBER 12 15 DECEMBER 1980

Structural study of stage-1 cesium graphite at high temperatures*

N. Caswell†
The James Franck Institute and the Department of Physics, University of Chicago, Chicago, Illinois 60637
(Received 4 March 1980)

New x-ray-diffraction results on the high-temperature structure of state-1 Cs graphite as a function of sample temperature and Cs-vapor pressure are presented. It is shown that the dominant factor in determining the high-temperature structure is the concentration of Cs atoms. An order-disorder transition occurs when the saturated compound C_8Cs decomposes. The decomposition occurs in two steps. The sample first transforms from the 300-K ordered phase with $\alpha\beta\gamma$ stacking to an unstable ordered phase with $\alpha\beta$ stacking. Then the sample undergoes an order-disorder transition to a phase with "liquidlike" planar structure. Also presented is evidence for the existence of an $\alpha\beta\gamma\delta$ stacking sequence in stage-1 Cs graphite at 300 K.

I. INTRODUCTION

As has been known for some time, a wide variety of chemical species enter the interlayer space of graphite to form graphite intercalation compounds (GIC).[1] Some species, in particular the alkali metals[2] K, Rb, and Cs, form "pure-stage" GIC's in which the intercalant layers form a regular array, each pair separated by exactly N carbon layers.[3] The integer N, referred to as the stage, partially characterizes the compound. The structure and stoichiometry of the intercalant layers and any correlations between the layers must also be specified.

For stage N, $N \geq 2$, alkali-metal GIC's the stoichiometry is $C_{12N}M$, $M = K, Rb, Cs$. At 300 K the metal layers are disordered and there are no correlations between layers.[4] At a temperature below room temperature the metal layers undergo an order-disorder transition (ODT) as first demonstrated by Parry and co-workers.[5] Recent results by Clarke, Caswell, and Solin (CCS)[4] for stage-2 Cs graphite have shown that the Cs atomic positions in the disordered Cs layers have the short-range order of a triangular lattice with the Cs atoms unregistered with the underlying graphite lattice. At the ODT the cesium atoms freeze into an incommensurate triangular lattice, modulated by the graphite potential.

The situation in the stage-1 alkali-metal GIC's is radically different. The stoichiometry of the stage-1 compounds is C_8M, $M = K, Rb, Cs$, and represents the saturation concentration of the alkali metal in the graphite lattice. At ambient pressure and room temperature the stage-1 compounds are three-dimensionally ordered, forming a superlattice with respect to the graphite lattice.[6] There exist[7,8] relatively little data on the phase transition which is known to occur at high temperatures although a theoretical prediction that the transition should be first order in C_8Cs and C_8Rb exists.[9]

Ellenson *et al.*[7] made neutron diffraction measurements on C_8Rb at several temperatures. They reported two new structural phases: an ordered, "$\alpha\beta$" phase at 708 K with a lattice constant in the direction perpendicular to the graphite layer plane one-half its room-temperature value; and a disordered phase at 747 K signaled by the disappearance of the Bragg reflections due to the long-range order of the Rb atoms.

Clarke, Caswell, and Solin[8] (CCS) using x-ray diffraction observed an ODT in stage-1 Cs graphite at 608 K in a sample whose ampoule contained excess Cs metal to maintain a saturated vapor. On the basis of the measured liquid structure factor (LSF) CCS argued that at temperatures above the ODT the Cs atoms formed liquidlike layers with atomic positions uncorrelated with the graphite lattice. The average Cs–Cs distance in the disordered layer was slightly greater than in the ordered phase, indicating Cs was expelled on melting and re-entered from the vapor on freezing. A second, "nonexcess" sample, the ampoule of which contained no excess of Cs metal, showed different behavior, demonstrating the importance of the Cs-vapor environment. Cesium expelled on the first melting of the ordered structure was not replaced on freezing, causing the room-temperature structure to be a phase-separated mixture of stage-1 and stage-2 compounds. The stage-1 regions of this mixture melted at 503 K, transforming the sample to a uniform stage-1 phase with lattice-gas structure in the Cs layers.

Salzano and Aronson (SA) have published a series of papers on the thermodynamic properties of the alkali-metal GIC's.[10-14] From decomposition-rate and vapor-pressure data, SA infer the existence of a compound with stoichiometry $C_{10}M$, $M = K, Rb, Cs$, between the more commonly recog-

nized C_8M and $C_{24}M$, $M=K,Rb,Cs$, stoichiometries.[14] As SA have noted,[10] the $C_{10}Cs$ compound, identified by its enthalpy and entropy of formation and decomposition, does not have the exact stoichiometry $C_{10}Cs$ but is in fact stable over a range of stoichiometries C_nCs, $9<n<11$.

The present work expands the previous investigations of stage-1 Cs graphite. In particular, the thermodynamic information of SA[11,12] is coupled with the indication of variable Cs-layer concentration from CCS[8] to provide an understanding of the temperature, Cs vapor pressure, and Cs-layer concentration dependence of the high-temperature structure and ODT. As will be seen in Sec. IV, the ODT is not a simple structural phase transition, but a transformation between chemically similar compounds.

The transition is observed to proceed in two steps. First, a stacking sequence transition from the RT phase to an ordered phase analogous to the $\alpha\beta$ phase seen by Ellenson *et al.*[7] in Rb graphite occurs. Second, the $\alpha\beta$ phase undergoes an ODT to the liquidlike phase observed by CCS.[8] The structural transition occurs at the sample temperature T_s and cesium vapor pressure P_{Cs} measured by SA[10-12] for the decomposition of C_8Cs. The structure of the disordered phase is discussed in Sec. V, where it is shown that the disordered phase cannot be a lattice gas, although effects due to the graphite lattice are observable.

Prior to the discussions of Secs. IV and V, Sec. II will describe the experimental apparatus and procedures. Section III deals with the ordered structure of stage-1 Cs graphite. The accepted C_8Cs, 300-K structure[6] was observed. However, a new unstable phase having a Cs-layer stacking sequence with a repeat distance of four Cs-layer spacings in the direction perpendicular to the graphite planes is shown to exist. The new structure decays into the accepted structure on a time scale of days.

II. EXPERIMENTAL PROCEDURES

A. Sample preparation

Samples were prepared from highly oriented pyrolytic graphite (HOPG) pieces $10\times6\times0.3$ mm^3. These were cut from larger slabs using a wire saw and 600 SiC grit. The graphite was cleaned with acetone then rinsed in distilled and deionized water, after which it was cleaved to the desired thickness using a razor blade. The final surface was exposed by peeling thin layers off with Scotch tape. High-quality surfaces were obtainable by this method.

Sample holders as shown in Fig. 1(a) were prepared from Pyrex tubing. To minimize background x-ray scattering from the glass the region around the sample was etched to a thickness of 0.2 mm using hydrofluoric acid, (HF).[15] The holders were loaded with graphite and cesium (alpha inorganic 99.99%) under a helium atmosphere then evacuated and sealed at 10^{-4} Torr. The Cs was distilled *in situ* to purify the metal and to remove any residual reactive gasses by reaction with the Cs vapor. The residue was sealed and removed, leaving the sample holder with graphite and Cs as shown in Fig. 1(a).

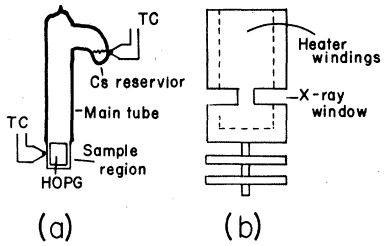

FIG. 1. (a) Sketch of the Pyrex sample holder containing Cs in the sidearm and an HOPG sample in the sample region. Temperatures were measured at the points labeled "TC". (b) Sketch of the Lavite oven used to heat the sample region.

B. Techniques

Independent control of the Cs vapor pressure P_{Cs} and sample temperature T_s was accomplished by two-zone heating of the sample holder. The Cs in the reservoir maintained the system at a vapor pressure determined by the reservoir temperature T_{Cs} set by heater coils wrapped on the sidearm and main-tube portion. The sample was heated by inserting the sample region into a separate sample oven, shown in Fig. 1(b), constructed from Lavite and mounted on a universal goniometer to couple with the x-ray diffractometer.

Temperatures were measured using chromel-alumel thermocouples. The possibility of temperature gradients in the sample region due to heat loss through the oven windows was carefully considered. Tests with multiple thermocouples in contact with the outside of the sample holder near the sample edge and insulated from the ambient atmosphere showed a maximum variation of 5 K at 700 K. An uninsulated thermocouple placed close to the glass in the oven window indicated a temperature 20 K lower than the temperature near the sample edge. Since the sample edges were insulated from the atmosphere and intercalated graphite is metallic[16] (and therefore a good heat conductor) while the glass holder is not, the temperature near the sample edge was taken as the sample temperature.

The Cs reservoir temperature was measured

at the tip of the sidearm which was verified to the point of lowest temperature by multiple thermocouple tests and observing that the Cs in the system always condensed there. Temperatures measured near the sidearm tip showed a variation of <3 K while the temperature along the main tube and at the top of the sample holder was >20 K above the temperature of the sidearm tip. The sample region was always maintained at a temperature higher than that of the Cs reservoir. The measured temperatures had a precision of ±1 K, not including a possible systematic error of 5 K. Temperature stability was better than ±2 K.

The Cs vapor pressure was calculated from thermodynamic data[17] using the relation

$$-\ln\frac{P_{Cs}}{P_0}=\frac{\Delta H_v}{RT_{Cs}}-\frac{\Delta S_v}{R}, \tag{1}$$

where ΔH_v and ΔS_v are the molar change in enthalpy and entropy on vaporization, T_{Cs} is the temperature of the reaction Cs (liquid)$\rightleftharpoons$Cs (gas), P_0 is the pressure of a standard state chosen to be 1 atm, and R is the gas constant. The quantities ΔH_v and ΔS_v tabulated in Ref. 17 are weak functions of temperature. However, the variation is small over the temperature range of 320 $< T_{Cs} <$ 550 K, so the average values $\Delta H_v = 17.9$ kcal/mole and $\Delta S_v = 18.2$ cal mole^{-1}K^{-1} were used to calculate P_{Cs}.

In order to compare varying Cs superstructures and exhibit their relation to the underlying graphite lattice, it will be convenient to label the scattering vector $\vec{q}$, $|q| = 4\pi\sin\theta/\lambda$, by the indices h,k,l of a reference unit cell fixed by the graphite lattice. The reference unit cell shown in Fig. 2 has lattice vectors $2\vec{a}_1$ and $2\vec{a}_2$($|\vec{a}_1| = |\vec{a}_2| = a$) in the graphite plane, where $\vec{a}_1$ and $\vec{a}_2$ are the in-plane lattice vectors of pristine graphite, and a lattice vector $\vec{c}$ perpendicular to the graphite plane with a magnitude equal to the separation between adjacent Cs layers. Any scattering vector $\vec{q}$ may be written

$$\vec{q} = h\vec{a}_1^* + k\vec{a}_2^* + l\vec{c}^*, \tag{2}$$

where h,k,l, are continuous variables and a_1^*, a_2^*, c^* are reciprocal-lattice vectors.

The HOPG used in this experiment is a polycrystalline material with the $\vec{c}$ axes of the microcrystals parallel with some mosaic spread and the $\vec{a}_1$ and $\vec{a}_2$ axes randomly oriented. Crstallographically HOPG appears as a single crystal perpendicular to the graphite planes and as a powder in the planes. Because the powder averaging of the h and k indices results in rings of intensity in the (hk) plane with cylindrical symmetry around $\vec{c}^*$, a scan along any line with constant l passing through the point $h=0$, $k=0$, passes through rings

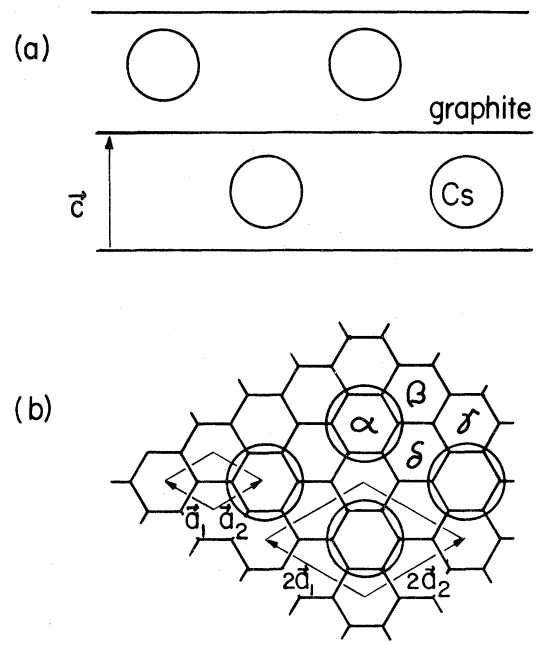

FIG. 2. (a) A c-axis section of stage-1 Cs-graphite with Cs atoms located between graphite layers. (b) A region of the graphite plane showing pristine graphite lattice vectors $\vec{a}_1$, $\vec{a}_2$, reference unit-cell lattice vectors $2\vec{a}_1$, $2\vec{a}_2$, locations and approximate radius of Cs atoms on α sites, and the β, γ, and δ sites.

for every h and k index. Accordingly a single index h' will be used:

$$h' = |h2\vec{a}_1 + k2\vec{a}_2|. \tag{3}$$

For simplicity of notation the prime will be dropped, and the in-plane powder index referred to as "h." A general point in reciprocal space will be referred to by the ordered pair (h,l). The scattering geometries used are shown in Figs. 3(a)–3(c).

The sample stage is determined by scanning in the $(0,l)$ direction from $25° < 2\theta < 40°$. All diffraction data presented here are for stage-1 samples in which no evidence of stage-2 $(0,l)$ reflections could be found. Diffraction measure-

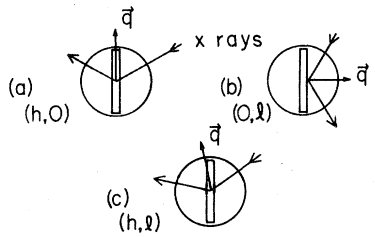

FIG. 3. (a)–(c) Diffraction scattering geometries for $(h, 0)$, $(0, l)$, and (h, l) reflections, respectively. [See text for description of (h, l) notation.]

ments were carried out on a Picker FACS-I diffractometer with a Rigaku 12 kW rotating-anode x-ray generator using graphite (002)-monochromated Mo $K\alpha$ radiation.

As will be seen in Sec. IV below, the concentration of Cs atoms in each layer is an important quantity. The Cs concentration is measured by comparing the linear attenuation coefficient of the Cs for a sample of arbitrary concentration, μ_{Cs}, with the linear attenuation coefficient for a sample of known concentration, μ^0_{Cs}. Since μ_{Cs} is proportional to the Cs concentration, we may define the relative concentration C as

$$C \equiv \mu_{Cs}/\mu^0_{Cs} . \tag{4}$$

The saturated compound C_8Cs is used as the standard, so $0 \leq C \leq 1$, where $C=0$ represents pristine graphite.

The x-ray intensity I (C,ϕ) reaching the detector for a source intensity I_s is

$$I(C,\phi) = I_s \exp\{-[\mu_{Cs}(C) + \mu_g]\sec(\phi)t - \alpha\}, \tag{5}$$

where ϕ is the angle between the sample c axis (which is perpendicular to the sample face) and the incident x-ray beam, μ_g is the linear absorption coefficient of the graphite, t is the thickness of the sample, and α contains factors for all other absorbers, such as the sample holder glass and air, in the beam path. The quantity $(\mu_{Cs} + \mu_g)t$ is obtained from the intensity ratio $I(1,\phi)/I(1,0)$:

$$(\mu^0_{Cs} + \mu_g)t = (1 - \sec\phi)^{-1} \ln \frac{I(1,\phi)}{I(1,0^\circ)} . \tag{6}$$

Since μ^0_{Cs} and μ_g can be calculated from the known mass densities of Cs and carbon in C_8Cs and the known mass absorption coefficients for Cs and carbon,[17] Eq. (6) represents a determination of the unknown t.

The thickness t determined in this way is the optical thickness which is insensitive to macroscopic flaws in the sample such as cracks or voids which would affect a mechanical measurement. The optical thickness for a typical sample determined by the procedure outlined here was 0.323 ± 0.005 mm while the mechanical thickness measured by viewing the sample edge with an eyepiece and graticule was 0.3 ± 0.05 mm. An unknown Cs concentration may now be determined from the intensity ratio

$$\frac{I(C,0^\circ)}{I(1,0^\circ)} = \exp\{-[\mu_{Cs}(C) - \mu^0_{Cs}]t\},$$

or using Eq. (4)

$$C = 1 - \frac{1}{\mu^0_{Cs}t} \ln\left(\frac{I(C,0^\circ)}{I(1,0^\circ)}\right) . \tag{7}$$

The dimensionless quantity $\mu^0_{Cs}t$ was measured to be 2.3 ± 0.05 for the primary sample used in this study. The total uncertainty in C due to the uncertainty in $\mu^0_{Cs}t$ and fluctuations in the source x-ray intensity is estimated to be $\lesssim 4\%$.

III. ROOM-TEMPERATURE RESULTS

The ideal structure of C_8Cs is shown in Fig. 2.[6] Carbon planes stacked along the $\vec{c}$ axis are equivalent, forming an A-A-$A\cdots$ sequence. Within each Cs layer the Cs atoms form a $2\vec{a}\times 2\vec{a}$ superlattice commensurate with the graphite net. There are four possible origins for the $2\vec{a}\times 2\vec{a}$ intercalant lattice, labeled α, β, γ, and δ in Fig. 2(b). In C_8K and C_8Rb the $\vec{c}$-axis repeat distance is $4|\vec{c}|$, where $\vec{c}$ is defined in Sec. II above, with the metal layer stacking sequence being some permutation of $\alpha\beta\gamma\delta$. This stacking sequence of ordered $2\vec{a}\times 2\vec{a}$ Cs layers will be referred to as the $\alpha\beta\gamma\delta$ structure. C_8Cs is unique in that for the reported[6] room-temperature structure the $\vec{c}$-axis repeat distance is $3|\vec{c}|$, with the stacking sequence $\alpha\beta\gamma$. This stacking sequence of ordered $2\vec{a}\times 2\vec{a}$ Cs layers will be referred to as the $\alpha\beta\gamma$ structure.

A stage-1 sample with the $\alpha\beta\gamma$ structure was prepared by heating a saturated C_8Cs sample to above the melting transition discussed in Sec. IV below, cooling and maintaining the sample at $T_s = 570$ K and $P_{Cs} = 0.1$ Torr for 5 h, then cooling and maintaining the sample and metallic Cs at 300 K for 15 d. Figure 4 contains several traces along the indicated lines in reciprocal space. The $\alpha\beta\gamma$ structure is evident from peaks at $(1,\frac{1}{3})$ and $(1,\frac{2}{3})$ in Fig. 4(b). The width of the peaks in the $(1,l)$ and $(2,l)$ scans is consistent with the measured mosaic spread [4°, full width at half maximum (FWHM)] and the width in $(h,0)$ is consistent with the instrument (0.4°, FWHM).

Figure 5(a) shows a $(1,l)$ scan on the same immediately after cooling to 300 K. A new peak is present at $(1,\frac{1}{2})$ and the peaks at $(1,\frac{1}{3})$ and $(1,\frac{2}{3})$ are shifted towards $l=0$ and 1, respectively. The result of subtracting the $(1,l)$ scan of the $\alpha\beta\gamma$ structure, Fig. 4(b), from the $(1,l)$ scan of Fig. 5(a) is the pattern in Fig. 5(b). This pattern, with peaks at integer multiples of $\frac{1}{4}$, indicates a $4|\vec{c}|$ repeat distance. Furthermore, the $(1,0)$ and $(1,1)$ reflections are absent, consistent with structure factor calculations for an arbitrary stacking-sequence permutation of the $\alpha\beta\gamma\delta$ structure. It is concluded that stage-1 C_8Cs contains a previously unobserved admixture of the $\alpha\beta\gamma\delta$ structure.

To estimate the fraction of the $\alpha\beta\gamma\delta$ structure present in a mixed-phase sample the squares of the structure factors, $F^2(h,l)$, for the $(1,\frac{1}{4})$ and

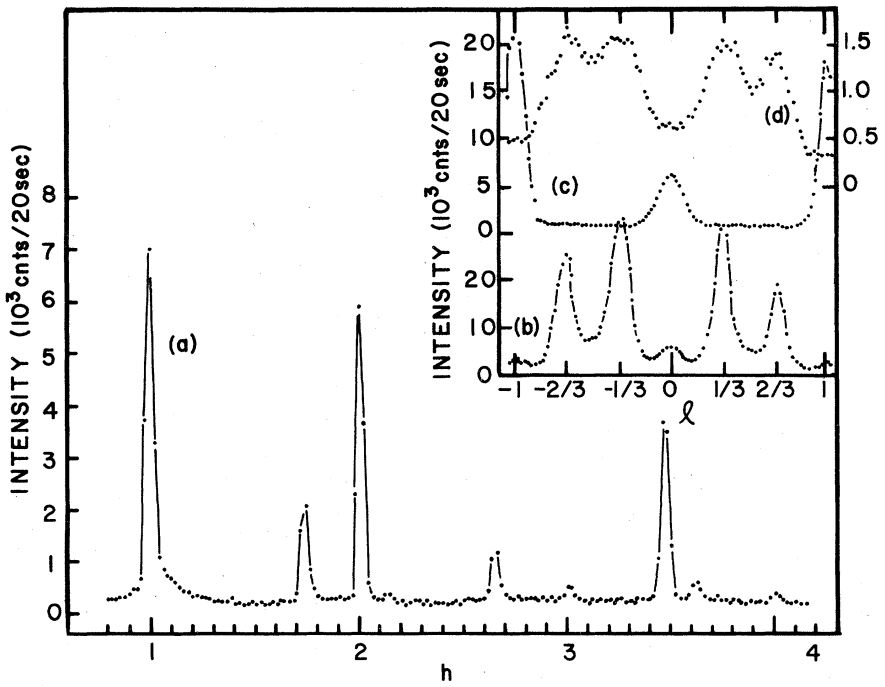

FIG. 4. 300 K diffraction patterns for C_8Cs. (a) $(h, 0)$ scan showing reflections at $2a$ positions. (b)–(c) (h, l) scans for $h = 1, 2, 3$, respectively, showing $3|\vec{c}|$ periodicity along the c axis. The reflections $(2, \frac{1}{3})$ and $(2, \frac{2}{3})$ are forbidden.

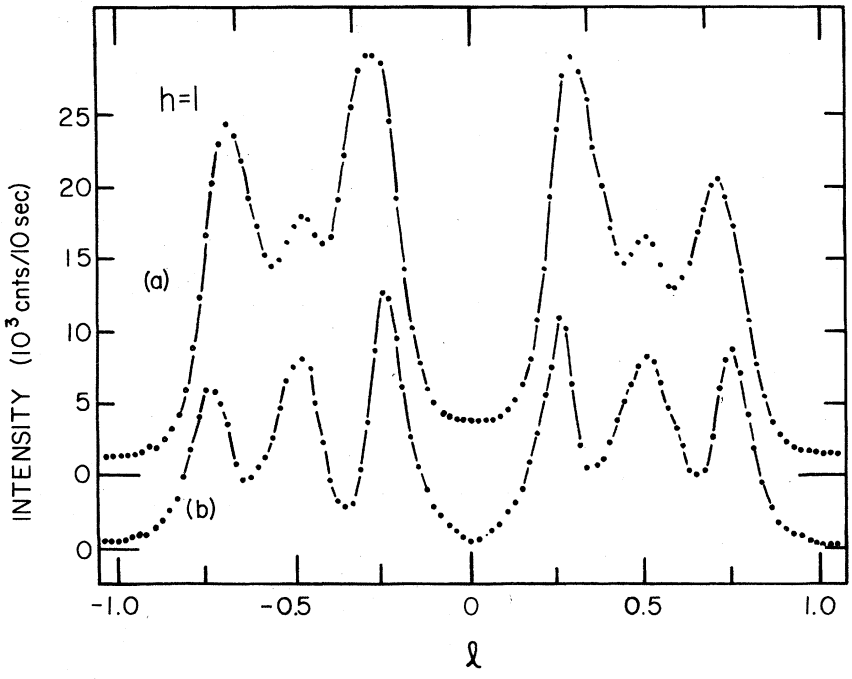

FIG. 5. 300 K diffraction pattern in $(1, l)$ direction showing the extra feature at $l = 0.5$. (b) The result of subtracting the $(1, l)$ scan of Fig. 3(b) from the $(1, l)$ scan of Fig. 4(a) yielding the diffraction pattern of the $\alpha\beta\gamma\delta$ structure.

$(1,\frac{1}{3})$ reflections are required. Stacking sequences which are not related by cyclic permutations or inversions do not necessarily have the same structure factors for a particular reflection. In the $\alpha\beta\gamma$ structure all permutations are cyclic permutations or inversions, so only one set of $F^2(h,l)$ need be calculated. The $F^2(h,l)$ calculated for the $(1,\frac{1}{3})$ reflections is $\frac{1}{9}$. In the $\alpha\beta\gamma\delta$ structure there are three classes of permutations, represented by $\alpha\beta\gamma\delta$, $\alpha\gamma\beta\delta$, and $\alpha\gamma\delta\beta$. It is assumed that any permutation is equally likely. Since each class contains an identical number of members, $F^2(h,l)$ is obtained by averaging $F^2(h,l)$ for the three permutations above the equal weight. The $F^2(1,\frac{1}{4})$ computed by this procedure is $\frac{5}{12}$. With this information, the fraction of the $\alpha\beta\gamma\delta$ structure in the sample, f, is estimated from

$$\frac{I(1,\frac{1}{4})}{I(1,\frac{1}{3})}=\frac{F^2(1,\frac{1}{4})}{F^2(1,\frac{1}{3})}\frac{f}{1-f}\,, \tag{8}$$

where $I(h,l)$ is the intensity of the (h,l) reflection. From Fig. 5, $I(\frac{1}{4})/I(\frac{1}{3})=1\pm0.2$, so $f=0.21\pm0.06$. Note that the data from Figs. 4 and 5 are for the same sample at 300 K at different times. The $\alpha\beta\gamma\delta$ structure is not stable at 300 K but relaxes to the $\alpha\beta\gamma$ structure on a time scale of days. Since the relaxation time is long compared to the time required to collect the data in Fig. 5, these data are representative of some higher temperature. Two sources of the $\alpha\beta\gamma\delta$ structure are suggested. First, it is possible the mixture of stacking sequences is an equilibrium phenomenon implying the $\alpha\beta\gamma\delta$ structure is thermally excited from the $\alpha\beta\gamma$ structure. In this case the fraction of $\alpha\beta\gamma\delta$ structure present would be determined by the Boltzmann factor. Second, it is possible that the $\alpha\beta\gamma\delta$ structure is a metastable configuration resulting from rapidly cooling the high-temperature structure discussed in Sec. IV below. These mechanisms are not mutually exclusive.

Since C_8Cs exhibits mixed stacking, one may speculate that C_8Rb, which prefers the $\alpha\beta\gamma\delta$ structure, exhibits a similar phenomenon having some regions with the $\alpha\beta\gamma$ structure. This might explain the "disordered" 300-K $(1,l)$ structure obtained for C_8Rb by Ellenson *et al.*[7]

IV. HIGH-TEMPERATURE RESULTS

The high-temperature structure of the stage-1 Cs GIC is intimately related to the concentration C of Cs in the sample. The equilibrium Cs concentration is shown as a function of P_{Cs} for $T_s=748$ K in Fig. 6(a). Good agreement is observed between the current diffraction experiment [solid circles in Fig. 6(a)] and a radioactive tracer experiment performed by SA[10] [solid line in Fig. 6(a)]. Decomposition of the C_8Cs compound is observed at $P_{Cs}=0.27$ Torr, where at equilibrium C changes discontinuously from $C=1$ to $C\approx0.88$. SA observed, and it is confirmed here,

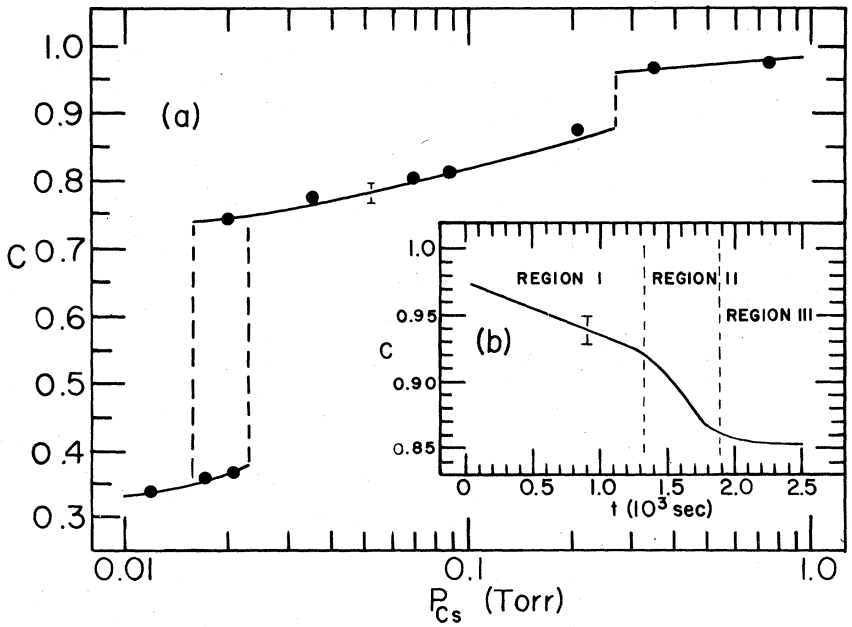

FIG. 6. (a) Equilibrium Cs concentration for $T_s=748$ K as a function of P_{Cs}. Circles (•) are from the present experiment, while the solid line is an experimental curve from Ref. 10. (b) Time dependence of the concentration jump at $P_{Cs}=0.27$ Torr.

that there is no measurable hysteresis in this transition.[10]

SA labeled the lower concentration phase by its approximate concentration, $C_{10}Cs$.[10] To avoid confusion from referring to a structure with variable concentration by a fixed concentration, the $C_{10}Cs$ phase shall hereafter be labeled the L phase in anticipation of its liquidlike Cs layer structure. The range of concentrations over which the L phase has been observed is $0.75<C<0.9$. Note that the L phase occurs in a stage-1 compound.

At $P_{Cs}=1.7\times10^{-2}$ Torr [see Fig. 6(a)] the sample decomposes into stage-2 $C_{24}Cs$. This transition was not studied, other than to confirm its existence. The time evolution of the concentration for P_{Cs} just below the transition is plotted in Fig. 6(b). A detailed discussion of this will be deferred temporarily while the locus of the transition point as a function of P_{Cs} and T_s is discussed.

The $P_{Cs}=0.27$-Torr transition in Fig. 6(a) corresponds to the order-disorder transition observed by CCS[8] in the "excess" sample which contained saturated Cs vapor. The phase transition occurs when the temperature-dependent vapor pressure of the sample $P_{C_8Cs}(T)$ exceeds P_{Cs}, and the sample decomposes via the empirical reaction

$$\frac{n}{n-8}C_8Cs \rightleftharpoons \frac{8}{n-8}C_nCs + Cs\ (\text{gas}), \tag{9}$$

where n is the number of carbon atoms in the product. For $P_{C_8Cs}(T_s)<P_{Cs}$ the reaction proceeds from right to left and Cs is absorbed by the sample until the saturated compound C_8Cs is formed. For $P_{C_8Cs}(T_s)>P_{Cs}$ the reaction proceeds from left to right and the sample loses Cs until the Cs concentration reaches a stable phase with vapor pressure $P_{C_nCs}(T_s)$ such that $P_{C_nCs}(T_s)\leq P_{Cs}$.

By the arguments leading to Eq. (1) above the temperature dependence of $P_{C_8Cs}(T_s)$ should be

$$-\ln\frac{P_{C_8Cs}(T_s)}{P_0}=\frac{\Delta H}{RT_s}-\frac{\Delta S}{R}, \tag{10}$$

where ΔH and ΔS are the enthalpy and entropy of reaction for Eq. (10) and obtained $\Delta H=43.7$ kcal/mole and $\Delta S=43.4$ cal mole^{-1} K^{-1}.

The inverse temperature $1/T_s$ at which structural changes occur is plotted versus $-\ln(P_{Cs})$ in Fig. 7. (The nature of the structural change will be discussed below.) The quantity $-\ln(P_{C_8Cs})$ calculated from Eq. (10) with SA's[11] values for ΔH and ΔS is plotted as a solid line in Fig. 7. As can be seen, the agreement between this line and the experimental points determined by x-ray diffraction is excellent.

Since the rate at which a composition change will occur is set by the slowest process in the system,

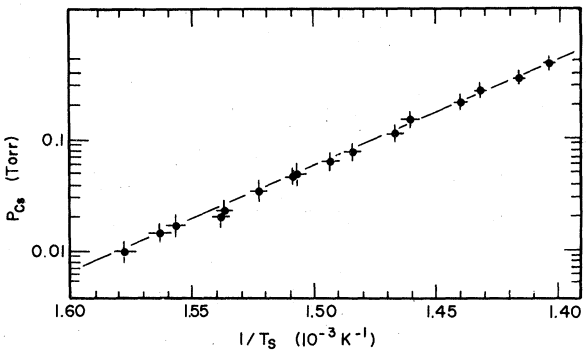

FIG. 7. Inverse temperature of structural transition in C_8Cs as function of $-\ln P_{Cs}$ (solid circles). The solid line is the equilibrium vapor pressure of C_8Cs from Ref. 11. Coincidence of these measurements indicate the structural change in C_8Cs is a result of decomposition rather than a structural phase transition.

in this case evaporation of the Cs atoms from the graphite surface,[11] the time to reach a compositionally stable phase may be long, as it is in Fig. 6(b).

Three regions are discernible in Fig. 6(b): region I in which C decreases slowly, region II in which it decreases rapidly, and region III in which C reaches its equilibrium value. Although region I can be prolonged for periods exceeding 12 h, C always decreases with time. This leads to the conclusion that the sample structure in region I is either unstable, or has a region of stability too narrow to be detected in this experiment.

An $(h,0)$ scan with the sample concentration in region I, Fig. 8(a), shows sharp peaks at the $2\vec{a}\times2\vec{a}$ positions although the intensities have changed markedly from the corresponding 300-K scan [Fig. 4(a)]. A new feature has appeared at $(0.5,0)$ indicating some admixture of a structure with an inplane $4|\vec{a}|$ periodicity, probably resulting from a modulation of the $2\vec{a}\times2\vec{a}$ lattice by cesium atom vacancies. No peaks at higher q corresponding to a $4|\vec{a}|$ periodicity, $(1.5,0)$, $(2.5,0)\ldots$ etc., are observed, although this is not surprising in view of the rapid falloff in intensity with increasing h of the peaks at the $2\vec{a}\times2\vec{a}$ positions as seen in Fig. 8(a).

The scans (h,l) for $h=1,2,3$ in Figs. 8(b)–8(d) show peaks at $(h,\frac{1}{2})$ indicating that the $\vec{c}$-axis repeat distance is $2|\vec{c}|$, where $\vec{c}$ is defined in Sec. II above. For $2\vec{a}\times2\vec{a}$ ordered Cs layers with $\alpha\beta$ stacking along the c axis the $(1,\frac{1}{2})$ reflection should be twice as intense as the $(1,0)$ reflection as it is in Fig. 8(b). The widths of the peaks in the (h,l) scans are consistent with the measured mosaic spread. This unstable structure corresponds to the intermediate phase found by Ellenson *et al.* for C_8Rb.[7] It will be referred to

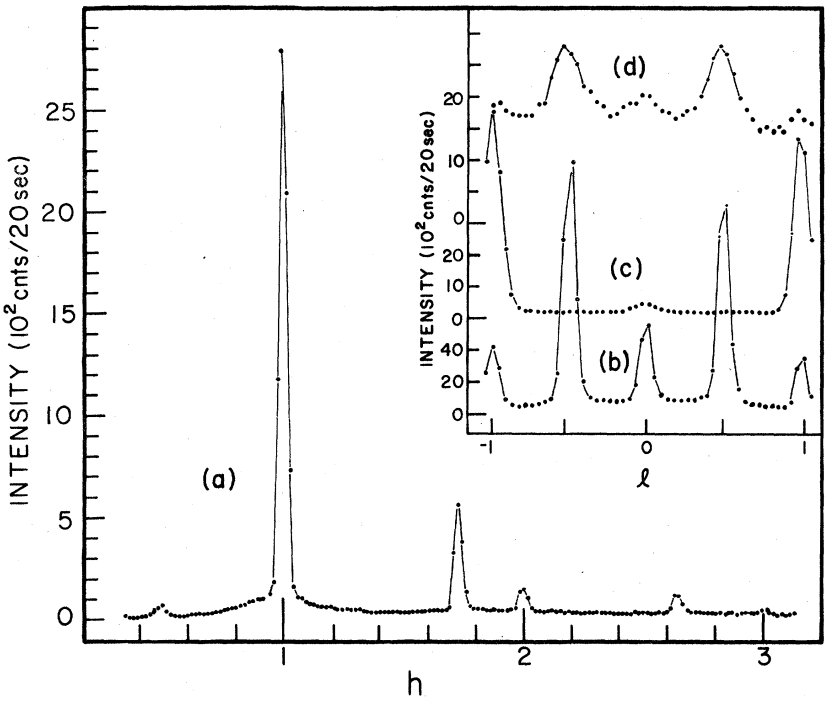

FIG. 8. (a) Diffraction patterns for the $\alpha\beta$ structure in the text. $(h, 0)$ scan showing reflections at $2a$ position, plus new feature at (0.50). (b)–(c) (h, l), $h = 1, 2, 3$, scans showing the $2|\vec{c}|$ periodicity along c axis.

as the "$\alpha\beta$ phase."

When the vacancy density reaches 8%, in region II, the rate of cesium loss increases. The intensity of the $2\vec{a}\times 2\vec{a}$ (1,0) reflection decreases to zero and a strong diffuse peak grows as the concentration drops to its equilibrium value in region III. The $(h,0)$ scans shown in Figs. 9(a)–9(c) exhibit the broad features characteristic of a disordered structure with superimposed reflections from the graphite layers at (2,0) and (4,0). The diffraction pattern along $(0.94, l)$ has a broad maximum at $l=\frac{1}{2}$ of width $\sim\frac{1}{2}$ due to short-range correlations between Cs positions in the $\vec{c}$ direction. From the width of the (0.94, 0.5) reflection and the Scherrer relation,[18] $L=2\pi/\Delta q$, where L is the correlation length and Δq is the width of the diffraction peak, a correlation length of approximately $2|\vec{c}|$ along the c axis is obtained. The most likely source of this correlation is a net repulsive interaction between Cs atoms in adjacent layers preventing them from occupying eclipsed positions. The origin of the repulsive interaction may be Coulombic,[19] elastic,[20] or both.

As mentioned above, the equilibrium concentration in the disordered phase is a function of P_{Cs} and T_s, varying from roughly $C=0.9$ to 0.75. If the atoms in each layer remain homogeneously distributed when C decreases, the average distance between first-nearest-neighbor cesiums, d_{NN} should increase with the ratio

$$d_{NN}^2/d_{0,NN}^2 = C_0/C\,, \tag{11}$$

where $d_{0,NN}$ is the Cs–Cs nearest-neighbor distance in the saturated compound C_8Cs. By definition, the saturated concentration $C_0=1$. A proper determination of d_{NN} in a system with nonisotropic three-dimensional correlations requires a knowledge of the scattering function $S(\vec{q})$ for all reciprocal space. However, for a close-packed structure an estimate of the nearest-neighbor distance may be obtained from the position of the first maximum in $S(q)$, q_{max}, using the Ehrenfest relation[21]

$$d_{NN} = K/q_{max} \tag{12}$$

or in the current notation $d_{NN}=Ka/h_{max}$, where h_{max} is the position of the first peak in $S(q)$, and K is a constant. For spherically isotropic materials, such as a liquid metal, $K=1.22$ is appropriate, while for cylindrically isotropic materials, such as the disordered phase of stage-2 Cs graphite,[4] $K=1.11$ is appropriate. For materials which are neither spherically nor cylindrically isotropic, an intermediate value for K may be used.[18] The d_{NN} calculated from the measured h_{max} with $K=1.18$ are shown in Fig. 10 along with the expected d_{NN} calculated from Eq. (11). Note that since K was chosen arbitrarily, Fig. 10 only

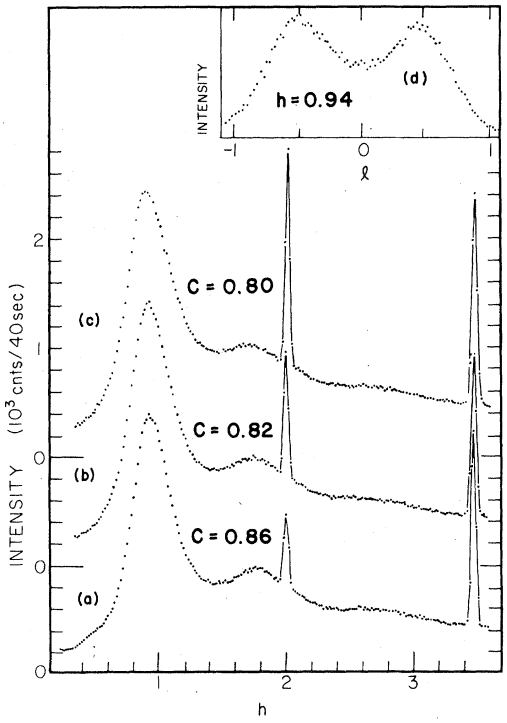

FIG. 9. Diffraction patterns of the L phase. (a)–(c) $(h, 0)$ scans of in-plane liquid structure factor for C = 0.86, 0.82, 0.80, respectively. (d) $(0.94, l)$ scan showing broad peaks at $0.5l$ indicative of short-range correlations along the c axis.

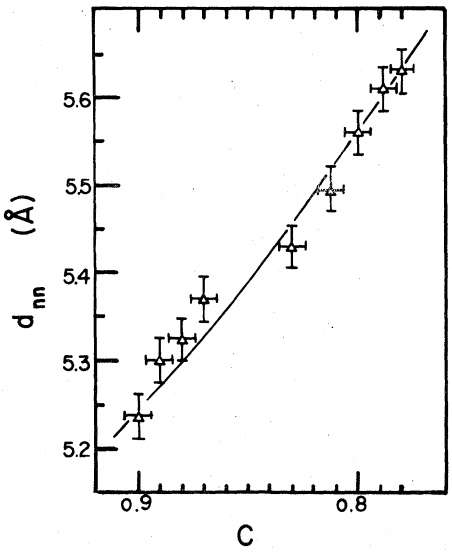

FIG. 10. Plot of Cs–Cs nearest-neighbor distance d_{NN} in the L phase estimated using the Ehrenfest relation with K = 1.18 (triangles). The solid line is the expected d_{NN} calculated from Eq. (13).

shows that d_{NN} has the correct functional dependence on concentration. Alternatively, if it is assumed d_{NN} must have the form of Eq. (11), Fig. 10 represents a determination of K.

V. DISCUSSION

Historically, discussions of the structure of alkali-metal GIC's have presumed that the alkali atoms are located over carbon prismatic sites.[22] This is almost certainly the case for the stage-1 ordered phases of Cs graphite in which the Cs atoms form a commensurate $2\vec{a}\times 2\vec{a}$ superlattice within each layer. As Cs atoms are removed from the saturated layer to form the disordered L phase, the Cs atoms may remain over the carbon prismatic sites. In this case, the disorder would be described by occupational disorder in a lattice gas. If the Cs atoms do not remain over the carbon prismatic sites the disorder would be described by positional disorder, as in liquid.

Note that the occurrence of the first maximum in the diffraction patterns of Fig. 10 at a $\vec{q}$ which is incommensurate with the graphite lattice does not immediately preclude a lattice-gas interpretation. The diffraction patterns of Fig. 10 are powder averaged around the c axis, so the observed peak may be the unresolved combination of peaks from several directions. In general the maximum of such a combination would occur at a position incommensurate with the graphite lattice. However, the diffraction patterns of Fig. 10 cannot be generated from a lattice-gas model, at the observed concentrations. This will be shown by a consideration of the width of the peak at $h \approx 0.94$.

When saturated, the Cs lattice gas forms the ordered $2\vec{a}\times 2\vec{a}$ superlattice. Because the size and mutual repulsion of the Cs atoms excludes occupation of the first- and second-neighbor lattice sites, isolated vacancies introduced into this structure do not affect the long-range order, as illustrated in Fig. 11(a). Excluded lattice sites are indicated by small dots in Fig. 11. The diffraction pattern from a Cs layer with only isolated vacancies would contain Bragg peaks at the $2\vec{a}\times 2\vec{a}$ positions. If the vacancies are collected in dislocation lines, the size of coherently diffracting $2\vec{a}\times 2\vec{a}$ regions will decrease and the width of the $h=1$ peak will increase. To estimate the minimum size of $2\vec{a}\times 2\vec{a}$ regions for a vacancy density, $\rho_v = 1 - C$, where C is the relative concentration, assume the sample consists of ordered $2\vec{a}\times 2\vec{a}$ regions of size $n\times n$ unit cells, with adjacent regions separated by dislocation lines with no isolated vacancies. Here n is any integer. From Fig. 11(b) it can be seen that along the dislocation line the unit cells of one region do not adjoin the unit cells of the adjacent region. The area of the vacant region is $\frac{1}{2}$ the unit cell area, implying that one

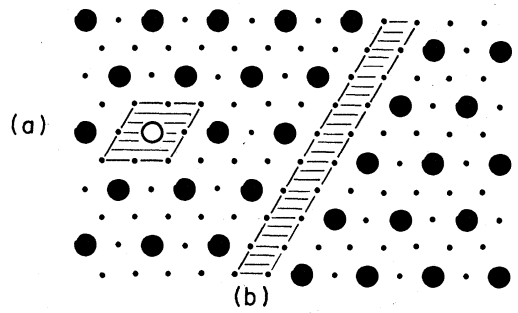

FIG. 11. Triangular lattice of graphite prismatic sites with • indicating a site occupied by a Cs atom, ○ indicating a site from which Cs is excluded by the Cs-Cs repulsion, and ○ an available but unoccupied site. (a) An isolated vacancy with no effect on the long-range order with shaded region showing the area of the empty unit cell. (b) A dislocation line showing the excess area not included in the unit cell net of either $2\vec{a}\times 2\vec{a}$ region.

vacancy is required for each 2 unit-cell lengths along the dislocation line. If neighboring regions contribute equally to producing the dislocation line, the number of vacancies an $n\times n$ unit-cell region must contain to enclose its perimeter with a dislocation line is $4n/4=n$. The number of vacancies available in an $n\times n$ unit-cell region is $\rho_v n^2$. The number required and the number available yield $n=1/\rho_v$.

At the highest concentration of the L phase, $C=0.9$, this calculation yields $n=10$. Thus for a unit-cell dimension of 4.97 Å, one expects $2\vec{a}\times 2\vec{a}$ regions of dimension 50 Å. Note that this estimate is low, since isolated vacancies and vacancy clusters larger than the dislocation line will enlarge the $2\vec{a}\times 2\vec{a}$ regions. Using the Scherrer equation [Eq. (3) above] regions this size would be expected to produce peaks at the $2\vec{a}\times 2\vec{a}$ Bragg positions, h an integer, with width $\sim 0.1h$. Instead, as can be seen in Figs. 10(a)–10(c), peaks of width $0.5h$ occur at $\sim(0.94,0)$. It is therefore concluded that the L phase is not a lattice gas but must have random positional disorder, similar to a liquid metal.

This conclusion is supported by the large vibrational amplitudes in the $\alpha\beta$ phase. The amplitude x can be calculated from the Debye-Waller factor,[18] which yields a value of $x=0.85\pm 0.1$ Å for the data of Fig. 8(a). The Lindemann melting formula[23] states empirically that a material will melt when the atomic vibrational amplitudes exceed some fraction f of the interatomic distance d, where f is between 0.2 and 0.25. The Lindemann limit for the $2\vec{a}\times 2\vec{a}$ structure, $2a=4.97$ Å, is between 1.0 and 1.25 Å, compared to an x of 0.85 ± 0.1 Å from the Debye-Waller measurement. By this qualitative criteria the $2\vec{a}\times 2\vec{a}$ layers in a sample with the $\alpha\beta$ structure are close to melting.

Although the Cs layers cannot be considered as a lattice gas, the graphite-Cs interaction is important. As the concentration decreases the effect of the Cs-Cs interaction will diminish relative to the graphite interaction. The graphite-Cs interaction will add a modulation with the long-range periodicity of the graphite lattice to the L-phase layers, resulting in a Cs contribution to the Bragg reflections at the graphite reciprocal-lattice points. Since the modulation increases as the relative effect of the graphite-Cs interaction increases, the intensity of the $(h,0)$ Bragg peaks, h an even integer, in the L phase should increase with decreasing Cs concentration. In Figs. 10(a)–10(c), the (2,0) reflection exhibits this behavior, while the (4,0) reflection does not. To understand this, the periodically modulated disordered structure may be thought of as a lattice with very large displacements from the equilibrium position. From this point of view one expects a very large Debye-Waller factor, explaining the enhancement of the (2,0) reflection while the (4,0) reflection intensity remains constant.

VI. SUMMARY AND CONCLUSION

It is important to note that the results presented here are for a particular type of sample environment, a constant vapor pressure externally imposed by an effectively infinite source and sink of Cs. This means the system will assume the stable phase with the highest concentration whose vapor is less than or equal to P_{Cs}. Ideally, one would like to study compounds with constant layer concentration, free from the complications of kinetics. At high temperatures, with high vapor pressures, such measurements are difficult or impossible. Other arrangements such as fixing the total number of cesium atoms in the system are possible. This was the case in the "nonexcess" sample of CCs.[8] It may be possible in such systems to study the L or $\alpha\beta$ phases at concentrations other than those accessible in this study. However, as discussed by CCs[8] in the case of the nonexcess sample where the total number of atoms in the system was insufficient to saturate the graphite, the phase transition is between an inhomogeneous stage-1, stage-2 mixture and a homogeneous disordered stage-1 phase rather than between two homogeneous phases. Even if the macroscopic concentration remains constant, the transition will involve a local concentration change as the $2\vec{a}\times 2\vec{a}$ regions expand into the unoccupied stage-2 graphite interlayer spaces.[8]

In conclusion, this paper has presented several new results on stage-1 Cs graphite. The exis-

tence of an $\alpha\beta\gamma\delta$ stacking phase at 300 K is reported for the first time as is the existence of an $\alpha\beta$ stacking phase at elevated temperatures. The ODT previously reported[8] is associated with the decomposition of C_8Cs (Refs. 9–12) into a compound with lower Cs concentration. The decomposition reaction is seen to proceed through two steps: first with the $\alpha\beta\gamma$ phase transforming to the $\alpha\beta$ phase, and the $\alpha\beta$ phase then undergoing a structural phase transition to the disordered L phase. Finally, while it was shown that the disordered L phase cannot be a lattice gas, the graphite-Cs interaction is not negligible. Modulation effects on the L phase by the graphite lattice are observed.

ACKNOWLEDGMENTS

Special thanks are due to Professor S. A. Solin for his advice and support during the completion of this project. Useful discussions with Roy Clarke and N. Wada are gratefully acknowledged. Thanks are also due to the J. Pluth for technical assistance and H. W. Moore who provided the HOPG used in this study. This research was supported by ARO-DAAG29-79-C-0029.

---

*Presented as a thesis to the Dept. of Physics, The University of Chicago, in partial fulfillment of the requirements for the Ph.D. degree.

†Present address: Dept. of Physics, Univ. of California, Berkeley, Calif. 94720.

[1]For a general review see J. E. Fischer and T. E. Thompson, Phys. Today 31, 36 (1978).

[2]A. R. Ubbelohde and F. A. Lewis, *Graphite and its Crystal Compounds* (Clarendon, Oxford, 1960).

[3]For a discussion of pure staging see W. Metz and D. Holwein, Carbon 13, 87 (1975).

[4]R. Clarke, N. Caswell, and S. A. Solin, Phys. Rev. Lett. (in press); Physica 99B, 457 (1980).

[5]G. S. Parry and D. E. Nixon, Nature 216, 909 (1967); G. S. Parry, D. E. Nixon, K. M. Lester, and B. C. Levene, J. Phys. C., Ser. 2, 2, 2156 (1969).

[6]W. Rudorff and E. Schulze, Z. Anorg. Chem. 277, 156 (1954).

[7]W. D. Ellenson, D. Semmingser, D. Guerard, D. G. Onn, and J. E. Fischer, Mater. Sci. and Eng. 31, 137 (1977).

[8]R. Clarke, N. Caswell, and S. A. Solin, Phys. Rev. Lett. 42, 61 (1979).

[9]P. Bak and E. Domany, Phys. Rev. B 20, 2818 (1979).

[10]F. J. Salzano and S. Aronson, J. Inorg. Nucl. Chem. 26, 1456 (1964).

[11]F. J. Salzano and S. Aronson, J. Chem. Phys. 42, 1323 (1965).

[12]F. J. Salzano and S. Aronson, J. Chem. Phys. 43, 149 (1965).

[13]F. J. Salzano and S. Aronson, J. Chem. Phys. 45, 4551 (1966).

[14]F. J. Salzano and S. Aronson, J. Chem. Phys. 47, 2978

[15]J. Fischer, private communication.

[16]D. G. Onn, G. M. T. Foley, and J. E. Fischer, Mater. Sci. and Eng. 31, 271 (1977).

[17]D. R. Still and G. C. Sinke, Adv. Chem. Ser. 18, 73 (1956).

[18]H. P. Klug and L. E. Alexander, *X-ray Diffraction Procedure for Polycrystalline and Amorphous Materials*, second ed. (Wiley Interscience, New York, 1974).

[19]F. J. Salzano and S. Aronson, J. Chem. Phys. 45, 2221 (1966).

[20]S. Saffran and Hamann, Phys. Rev. Lett. 42, 1410 (1979).

[21]*International Tables for X-ray Crystalography* (Kynoch, Birmingham, 1962), Vol. III, p. 318.

[22]Y. N. Novikov and M. E. Vol'pin, Russ. Chem. Rev. 40, 733 (1971) and references therein.

[23]J. M. Ziman, *Principles of the Theory of Solids*, second ed. (Cambridge University Press, New York, 1972).